The next step iterates equation (0.37) averaging the reflected terrain radiation over a square box of 0.5 × 0.5 km. If equation (0.37) is used with $E_t = E_g$ then three iterations are usually sufficient to be independent of the start value of the terrain reflectance [5]. However, for highly reflective surfaces, e.g. snow, and high terrain view factors, more than three iterations are necessary, and a faster convergence of $\bar{\rho}_{terrain}^{(i)}$ can be achieved with a geometric series for the terrain reflected radiation E_t as proposed in [22]:

$$E_t^{(i)} = E_g \frac{\bar{\rho}_{terrain}^{(i-1)} V_t}{1 - \bar{\rho}_{terrain}^{(i-1)} \bar{V}_t} \tag{0.38}$$

The last step accounts for the adjacency effect (equation (0.33)).

If $\theta s, \theta n, \varphi s, \varphi n$ denote solar zenith angle, terrain slope, solar azimuth and topographic azimuth, respectively, the illumination angle β can be obtained from the DEM slope and aspect angles and the solar geometry:

$$cos\beta(x,y) = cos\theta_s \; cos\theta_n(x,y) + sin\theta_s \; sin\theta_n(x,y) \; cos\{\phi_s - \phi_n(x,y)\} \tag{0.39}$$

The illumination image $cos\beta(x, y)$ is calculated within S2AC and stored as a separate map. The diffuse solar flux on an inclined plane is calculated with Hay's model [27] taking also into account the binary topographic cast shadow factor b:

$$E_d^*(x,y,z) = E_d(z) \; [b \; \tau_s(z) \; cos\beta(x,y)/cos\theta_s + \{1 - b \; \tau_s(z)\} V_{sky}(x,y)] \tag{0.40}$$

4.9 Empirical BRDF correction

For many surface covers the reflectance increases with increasing solar zenith and / or viewing angle [30]. Scenes in mountainous regions often exihibit a large variation of terrain slopes, and thus bidirectional brightness variations for a certain surface cover, e.g. meadow or forest. This behaviour cannot adequately be eliminated with the Lambertian assumption. It leads to overcorrected reflectance values in faintly illuminated areas (having small values of $cos\beta$), see Figure 4-13 (left). The center part of this Figure shows the result of an empirical correction with a simple geometric function depending on the local solar zenith angle β as explained below. Obviously, some correction is needed to avoid a misclassification of these bright overcorrected areas. Several approaches have been pursuit to solve this problem:

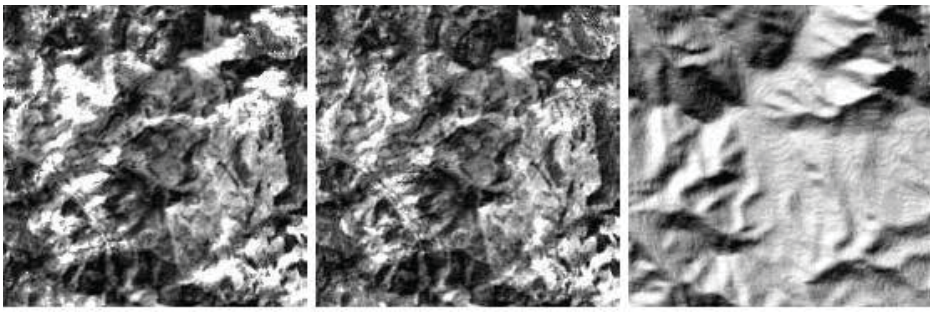

Figure 4-13 – BRDF correction in rugged terrain imagery
Left: image without BRDF correction.
Center: after BRDF correction with threshold angle βT = 65◦.
Right: illumination map = cos β

an empirical coefficient C is calculated based on a regression of brightness values and the local ilumination angle derived from the DEM. The coefficient depends on scene content and wavelength ([31], [32]).

the sun-canopy-sensor (SCS) geometry is employed in forested terrain instead of the solely terrain-based geometry [33].

the SCS method is coupled with the C-correction [34].

a simplified empirical approach accounting for the direct and diffuse illumination and incidence and exitance angles applied to vegetation canopies [35].

These approaches produced good results on sample scenes with uniform cover types presented in the above papers. When applying the methods to a wider range of areas, some of the practical problems are:

mountainous scenes often contain a number of different covers, e.g., deciduous forest, coniferous forest, mixed forest, shrubs, meadow, rocks, etc.

the computation of the C coefficients for different surface covers would require a pre - classification.

the correlation obtained for the C coefficients is often less than 0.7, yielding unreliable results with this method.

These remarks are supported by reference [32]. These authors applied different correction approaches to a TM scene containing different cover types and noted that there is no optimum method for all cover types. A drawback of the Minnaert and empirical C-methods is that they do do not distinguish between the direct and diffuse solar illumination as opposed to the physically based approach of S2AC. Nevertheless, the latter approach also cannot avoid problems in faintly illuminated areas. Therefore, it is supplemented by an empirical method with three adjustable parameters (βT , *b*, and *g*) as explained below. This approach was tested on different rugged terrain scenes with vegetated and arid landscapes and usually yields satisfactory results. It reduces overcorrected reflectance values starting at a threshold local solar zenith angle βT greater than the scene's solar zenith angle θs. Equation (0.41) defines the implemented basic geometric correction function which depends on the local solar incidence angle (solar illumination βi) and the threshold angle β_T . The exponent b (= 1/3, 1/2, 3/4, or 1) is the second parameter and can be selected by the user. Some guidelines on the choice of b are discussed below. The third adjustable parameter is the lower bound g of the correction function, see Figure 4-14.

$$G = \{cos\beta_i / cos\beta_T\}^b \qquad \leq g \tag{0.41}$$

The threshold illumination angle β_T should have some margin to the solar zenith angle to retain the original natural variation of pixels with illumination angles close to the solar zenith angle. The threshold angle can be specified by the user and the following empirical rules are recommended:

$\beta_T = \theta_s + 20^\circ$ *if* $\theta_s < 45^\circ$

If $45 \leq \theta_s \leq 20^\circ$ then $\beta_T = \theta_s + 15^\circ$

If $\theta_s > 55^\circ$ then $\beta_T = \theta_s + 10^\circ$

These rules are automatically applied if $\beta_T = 0$, e.g., during batch processing.

The geometric function G needs a lower bound g to prevent a too strong reduction of reflectance values. Values of G greater than 1 are set to 1, and values less than the boundary g are reset to g. This means the processing works in the geometric regime from βT to 90◦and the updated reflectance is

$$\rho_g = \rho_L G \tag{0.42}$$

where ρ_L is the isotropic (Lambert) value.

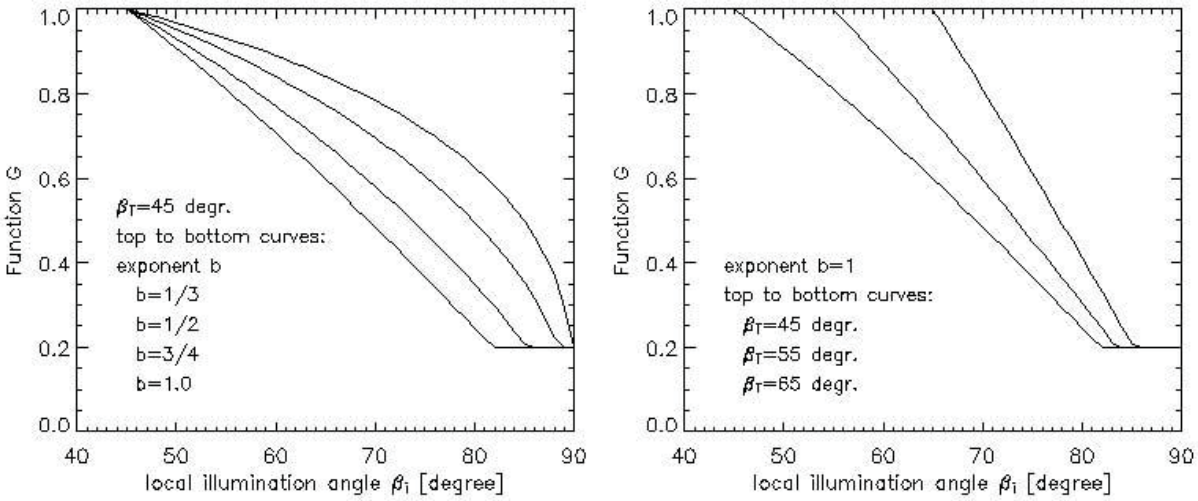

Figure 4-14 – Geometric functions for empirical BRDF correction

Left: Functions G of equation (0.41) for different values of the exponent b.
Right: Functions G of equation (0.41) for b=1 and different start values of βT.
The lower cut-off value is g=0.2.

Figure 4-14 shows a graphical presentation of equation (0.41). The left part displays the function G for different values of the exponent b. For b=1 the decrease with β_i is strong with a constant gradient. For smaller values of b the decrease with β_i is moderate initially, but the gradient increases with larger βi. Currently, different functions G for soil/sand and vegetation can be selected in S2AC [49]. The function G for soil / sand is applied with a wavelength-independent exponent b. After testing a large number of vegetated mountainous scenes two vegetation modes were finally selected because of their good performance:

1. b=0.75 for channels with λ< 720 nm and b=0.33 for λ> 720 nm (”weak” correction),

b=0.75 (λ< 720 nm) and b=1 (λ> 720 nm), (”strong” correction).

In most of the tested cases, the first vegetation mode (”weak” correction) was appropriate. A simple criterion (vegetation index ρ850nm/ρ660nm > 3) is used to distinguish soil/sand and vegetation. The right part of Figure 4-14 shows the effect of shifting the threshold illumination angle β_T . For larger values of β_T the decline of function G starts later with a larger gradient, and the lower bound g is met at slightly higher values of βi. In most cases, g=0.2 to 0.25 is adequate, in extreme cases of overcorrection g=0.1 should be applied.

Reference [7] contains a comparison of different topographic correction methods for several Landsat-TM, ETM+, and SPOT-5 scenes from different areas. The proposed empirical S2-AC approach performed best in most of these cases, but no method ranked first in all cases.